SOLUTIONS OF THE EULER EQUATIONS USING IMPLICIT TVD HIGH RESOLUTION ALGORITHMS IN THREE-DIMENSIONS

Edisson Sávio de Góes Maciel

edissonsavio@yahoo.com.br
Mechanical Engineer / Researcher
Rua Demócrito Cavalcanti, 152 – Afogados – Recife – PE – Brazil – 50750-080

Keywords: Steger and Warming algorithm, Van Leer algorithm, Implicit and TVD schemes, MUSCL procedure, Flux vector splitting.

Abstract. In the present work, the Steger and Warming and the Van Leer schemes are implemented, on a finite volume context and using a structured spatial discretization, to solve the Euler equations in the three-dimensional space. The Steger and Warming and the Van Leer schemes are flux vector splitting ones and in their original implementation are first order accurate. A MUSCL approach is implemented in these schemes aiming to obtain second order spatial accuracy. The Minmod non-linear limiter is employed to guarantee such accuracy and TVD high resolution properties. Both schemes are implemented following an implicit formulation. The flux vector splitting schemes employ approximate factorizations in ADI form. Both schemes are first order accurate in time. The algorithms are accelerated to the steady state solution using a spatially variable time step procedure, which has demonstrated effective gains in terms of convergence rate, as shown in Maciel. Both schemes are applied to the solution of the physical problems of the supersonic flow along a ramp and the "cold gas" hypersonic flow along a diffuser. The results have demonstrated that the most accurate results are obtained with the Steger and Warming TVD high resolution scheme.

1. INTRODUCTION

Conventional non-upwind algorithms have been used extensively to solve a wide variety of problems (Kutler, 1975, and Steger, 1978). Conventional algorithms are somewhat unreliable in the sense that for every different problem (and sometimes, every different case in the same class of problems) artificial dissipation terms must be specially tuned and judicially chosen for convergence. Also, complex problems with shocks and steep compression and expansion gradients may defy solution altogether.

Upwind schemes are in general more robust but are also more involved in their derivation and application. Some upwind schemes that have been applied to the Euler equations are: Roe (1981), Steger and Warming (1981) and Van Leer (1982). Some comments about these methods are reported below:

Roe (1981) presented a work that emphasized that several numerical schemes to the solution of the hyperbolic conservation equations were based on exploring the information obtained in the solution of a sequence of Riemann problems. It was verified that in the existent schemes the major part of these information was degraded and that only certain solution aspects were solved. It was demonstrated that the information could be preserved by the construction of a matrix with a certain "U property". After the construction of this matrix, its eigenvalues could be considered as wave velocities of the Riemann problem and the U_L-U_R projections over the matrix's eigenvectors would be the jumps which occur between intermediate stages.

Steger and Warming (1981) developed a method that used the remarkable property that the non-linear flux vectors of the inviscid gasdynamic equations in conservation law form were homogeneous functions of degree one of the vector of conserved variables. This property readily permitted the splitting of the flux vectors into subvectors by similarity transformations so that each subvector had associated with it a specified eigenvalue spectrum. As a consequence of flux vector splitting, new explicit and implicit dissipative finite-difference schemes were developed for first-order hyperbolic systems of equations.

Van Leer (1982) suggested an upwind scheme based on the flux vector splitting concept. This scheme considered the fact that the convective flux vector components could be written as flow Mach number polynomial functions, as main characteristic. Such polynomials presented the particularity of having the minor possible degree and the scheme had to satisfy seven basic properties to form such polynomials. This scheme was presented to the Euler equations in Cartesian coordinates and three-dimensions.

Second order spatial accuracy can be achieved by introducing more upwind points or cells in the schemes. It has been noted that the projection stage, whereby the solution is projected in each cell face *(i-½,i+½)* on piecewise constant states, is the cause of the first order space accuracy of the Godunov schemes (Hirsch, 1990). Hence, it is sufficient to modify the first projection stage without modifying the Riemann solver, in order to generate higher spatial approximations. The state variables at the interfaces are thereby obtained from an extrapolation between neighboring cell averages. This method for the generation of second order upwind schemes based on variable extrapolation is often referred to in the literature as the MUSCL ("Monotone Upstream-centered Schemes for Conservation Laws") approach. The use of non-linear limiters in such procedure, with the intention of restricting the amplitude of the gradients appearing in the solution, avoiding thus the formation of new extrema, allows that first order upwind schemes be transformed in TVD high resolution schemes with the appropriate definition of such non-linear limiters, assuring monotone preserving and total variation diminishing methods.

Traditionally, implicit numerical methods have been praised for their improved stability and condemned for their large arithmetic operation counts (Beam and Warming, 1978). On

the one hand, the slow convergence rate of explicit methods become they so unattractive to the solution of steady state problems due to the large number of iterations required to convergence, in spite of the reduced number of operation counts per time step in comparison with their implicit counterparts. Such problem is resulting from the limited stability region which such methods are subjected (the Courant condition). On the other hand, implicit schemes guarantee a larger stability region, which allows the use of CFL numbers above 1.0, and fast convergence to steady state conditions. Undoubtedly, the most significant efficiency achievement for multidimensional implicit methods was the introduction of the Alternating Direction Implicit (ADI) algorithms by Douglas (1955), Peaceman and Rachford (1955), and Douglas and Gunn (1964), and fractional step algorithms by Yanenko (1971). ADI approximate factorization methods consist in approximating the Left Hand Side (LHS) of the numerical scheme by the product of one-dimensional parcels, each one associated with a different spatial coordinate direction, which retract nearly the original implicit operator. These methods have been largely applied in the CFD community and, despite the fact of the error of the approximate factorization, it allows the use of large time steps, which results in significant gains in terms of convergence rate in relation to explicit methods.

In the present work, the Steger and Warming (1981) and the Van Leer (1982) schemes are implemented, on a finite volume context and using a structured spatial discretization, to solve the Euler equations in the three-dimensional space. The Steger and Warming (1981) and the Van Leer (1982) schemes are flux vector splitting ones and in their original implementation are first order accurate. A MUSCL approach is implemented in these schemes aiming to obtain second order spatial accuracy. The Minmod non-linear limiter is employed to guarantee such accuracy and TVD high resolution properties. Both schemes are implemented following an implicit formulation. The flux vector splitting schemes employ approximate factorizations in ADI form. Both schemes are first order accurate in time. The algorithms are accelerated to the steady state solution using a spatially variable time step, which has demonstrated effective gains in terms of convergence rate (Maciel, 2005 and 2008). Both schemes are applied to the solution of the physical problems of the supersonic flow along a ramp and the "cold gas" hypersonic flow along a diffuser. The results have demonstrated that the most accurate results are obtained with the Steger and Warming (1981) TVD high resolution scheme.

2. EULER EQUATIONS

The fluid movement is described by the Euler equations, which express the conservation of mass, of linear momentum and of energy to an inviscid, heat non-conductor and compressible mean, in the absence of external forces. In the integral and conservative forms, employing a finite volume formulation and using a structured spatial discretization, to three-dimensional simulations, these equations can be represented by:

$$\partial/\partial t \int_V Q dV + \int_S \left(E_e n_x + F_e n_y + G_e n_z \right) dS = 0, \tag{1}$$

where Q is written to a Cartesian system, V is a cell volume, which corresponds to an hexahedron in the three-dimensional space, n_x, n_y and n_z are the components of the normal unity vector pointing outward to the flux face, S is the surface area and E_e, F_e and G_e represent the components of the convective flux vector. Q, E_e, F_e and G_e are represented by:

$$Q = \begin{Bmatrix} \rho \\ \rho u \\ \rho v \\ \rho w \\ e \end{Bmatrix}, \quad E_e = \begin{Bmatrix} \rho u \\ \rho u^2 + p \\ \rho uv \\ \rho uw \\ (e+p)u \end{Bmatrix}, \quad F_e = \begin{Bmatrix} \rho v \\ \rho uv \\ \rho v^2 + p \\ \rho vw \\ (e+p)v \end{Bmatrix}, \quad G_e = \begin{Bmatrix} \rho w \\ \rho uw \\ \rho vw \\ \rho w^2 + p \\ (e+p)w \end{Bmatrix}. \tag{2}$$

The quantities that appear above are described as follows: ρ is the fluid density, u, v and w are the Cartesian components of the flow velocity vector in the x, y and z directions, respectively; e is the total energy per unity volume of the fluid; and p is the fluid static pressure.

The Euler equations were nondimensionalized in relation to the freestream density, ρ_∞, and the freestream speed of sound, a_∞, for the studied problems. To allow the solution of the matrix system of five equations to five unknowns described by Eq. (1), it is employed the state equation of perfect gases presented below:

$$p = (\gamma - 1)\left[e - 0.5\rho(u^2 + v^2 + w^2)\right], \tag{3}$$

where γ is the ratio of specific heats at constant pressure and volume, respectively, which assumed a value 1.4 to the atmospheric air. The total enthalpy is determined by:

$$H = (e + p)/\rho. \tag{4}$$

3. GEOMETRICAL CHARACTERISTICS OF THE SPATIAL DISCRETIZATION

Adopting in Equation (1) Q as a constant on a computational cell and using a structured mesh notation to the fluid and flow quantities, it is possible to write:

$$\partial Q_{i,j,k}/\partial t = -1/V_{i,j,k} \int_{S_{i,j,k}} (E_e n_x + F_e n_y + G_e n_z)_{i,j,k} \, dS_{i,j,k} \tag{5}$$

A given computational cell in this notation is composed by the following nodes: (i,j,k), (i+1,j,k), (i+1,j+1,k), (i,j+1,k), (i,j,k+1), (i+1,j,k+1), (i+1,j+1,k+1) and (i,j+1,k+1). Figure 1 shows a representation of the computational cell, which is a hexahedron in three-dimensions.
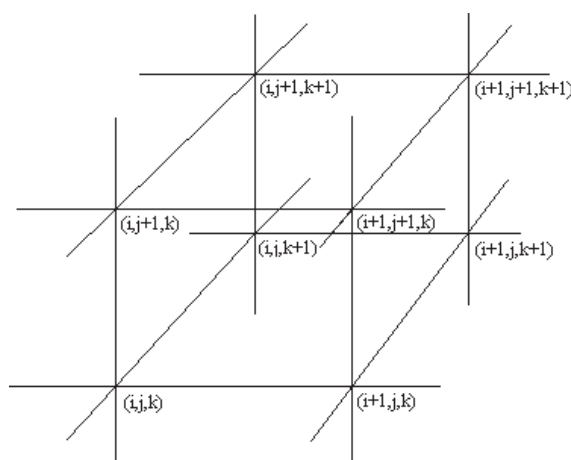
Figure 1: Computational cell to structured discretization.

The calculation of the volume of the computational cells is based, in the more general case, in the determination of the volume of a deformed hexahedron in the three-dimensional space. This volume is determined by the summation of the volumes of the six tetrahedrons which composes the given hexahedron. Figure 2 exhibits the division of a hexahedron in its six tetrahedral components, as well the nodes of the vertices which define each tetrahedron.
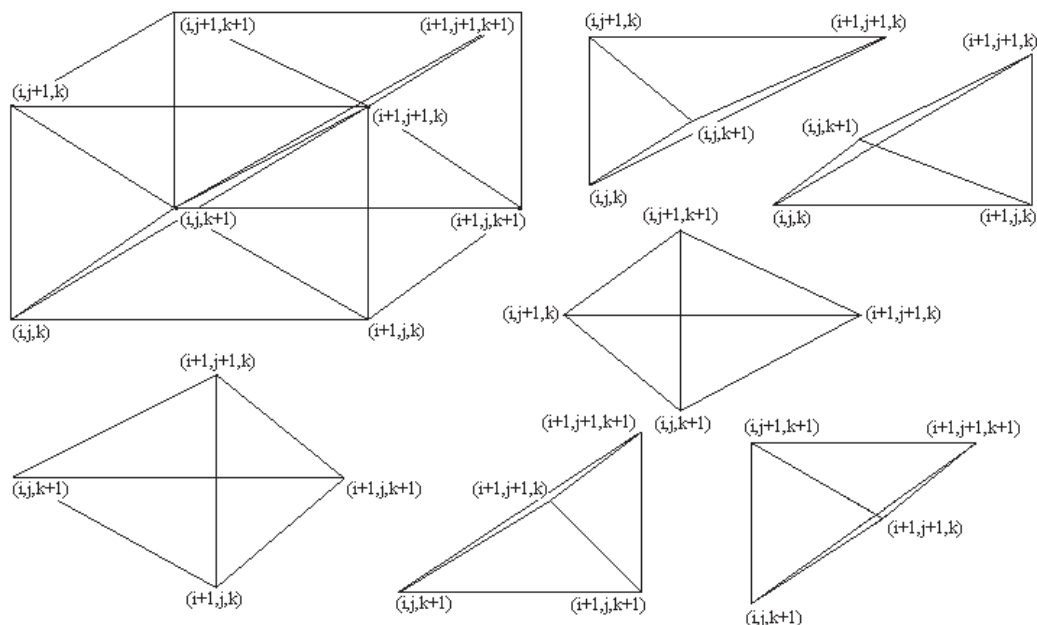
Figure 2: Definition of a hexahedron and its six tetrahedral components.

The volume of a tetrahedron is given by the calculation of the following determinant:

$$V_{PABC} = \frac{1}{6} \begin{vmatrix} x_P & y_P & z_P & 1 \\ x_A & y_A & z_A & 1 \\ x_B & y_B & z_B & 1 \\ x_C & y_C & z_C & 1 \end{vmatrix}, \tag{6}$$

where x_P, y_P, z_P, x_A, y_A, z_A, x_B, y_B, z_B, x_C, y_C and z_C are Cartesian coordinates of the nodes which define the tetrahedron represented in Fig. 3.
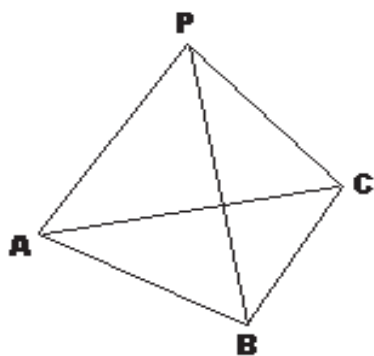
Figure 3: Reference tetrahedron.
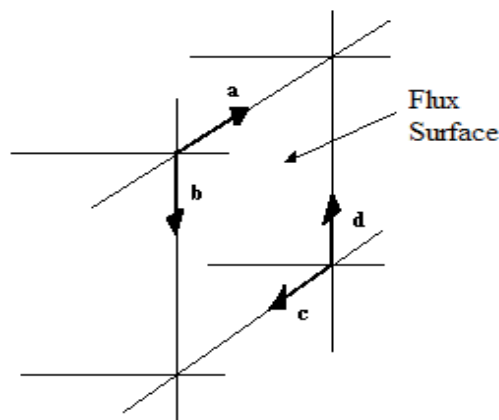
Figure 4: Flux area (hexahedron).

The flux area of the hexahedron is calculated by the sum of half areas defined by the vector external products $|\vec{a} \, x \vec{b}|$ and $|\vec{c} \, x \vec{d}|$, where $\vec{a}$, $\vec{b}$, $\vec{c}$ and $\vec{d}$ are vectors formed by the nodes which define a given flux surface, conform exhibited in Fig. 4. The physical quantity $0.5(|\vec{a} \, x \vec{b}| + |\vec{c} \, x \vec{d}|)$ determines the flux area of each face, which is nothing more than the area of a deformed rectangle.

The normal unity vector pointing outward at each flux face is calculated taking into account the vector external product $\vec{n} = \vec{a} \, x \vec{b} / |\vec{a} \, x \vec{b}|$, as shown in Fig. 5. An additional test is necessary to verify if this unity vector in point inward or outward of the hexahedron. This test is based on the following vector mixed product $[(\vec{a} \, x \vec{b}) / |\vec{a} \, x \vec{b}|] \bullet \vec{f}$, where $\vec{f}$ is the vector formed by one of the nodes of the flux face under study and one node of the hexahedron that be contained at the face immediately opposed, and "$\bullet$" represents the vector inner product. The positive signal indicates that the normal vector is pointing inward the hexahedron, what imposes that it should be changed by their opposed vector.
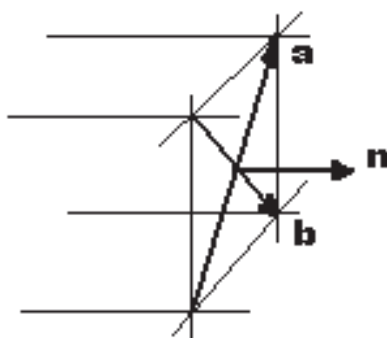
Figure 5: Normal unity vector (hexahedron).

4. NUMERICAL SCHEME OF STEGER AND WARMING (1981)

4.1 Theory for the one-dimensional case

If the homogeneous Euler equations are put in characteristic form

$$\partial W / \partial t + \Lambda \, \partial W / \partial x = 0 , \tag{7}$$

where W is the vector of characteristic variables (defined in Hirsch, 1990) and Λ is the diagonal matrix of eigenvalues, the upwind scheme:

$$u_i^{n+1} - u_i^n = -\Delta t / \Delta x \left[\hat{a}^+ \left(u_i^n - u_{i-1}^n \right) + \hat{a}^- \left(u_{i+1}^n - u_i^n \right) \right], \tag{8}$$

where u is a scalar property, $\hat{a}^+ = 0.5(\hat{a} + |\hat{a}|)$ and $\hat{a}^- = 0.5(\hat{a} - |\hat{a}|)$, can be applied to each of the three characteristic variables separately, with the definitions

$$\lambda_l^+ = 0.5(\lambda_l + |\lambda_l|) \quad \text{and} \quad \lambda_l^- = 0.5(\lambda_l - |\lambda_l|) \tag{9}$$

for each of the eigenvalues of Λ

$$\Lambda = \begin{bmatrix} \lambda_1 & & \\ & \lambda_2 & \\ & & \lambda_3 \end{bmatrix} = \begin{bmatrix} u & & \\ & u+a & \\ & & u-a \end{bmatrix}. \tag{10}$$

This defines two diagonal matrices $\Lambda^{\pm}$:

$$\Lambda^{\pm} = \begin{bmatrix} \lambda_1^{\pm} & & \\ & \lambda_2^{\pm} & \\ & & \lambda_3^{\pm} \end{bmatrix} = \begin{bmatrix} 0.5(u \pm |u|) & & \\ & 0.5(u+a \pm |u+a|) & \\ & & 0.5(u-a \pm |u-a|) \end{bmatrix}, \tag{11}$$

where Λ^+ has only positive eigenvalues, Λ^- only negative eigenvalues, and such that

$$\Lambda = \Lambda^+ + \Lambda^- \quad \text{and} \quad |\Lambda| = \Lambda^+ - \Lambda^- \quad \text{or} \quad \lambda_l = \lambda_l^+ + \lambda_l^- \quad \text{and} \quad |\lambda_l| = \lambda_l^+ - \lambda_l^-. \tag{12}$$

The quasi-linear coupled equations are obtained from the characteristic form by the transformation matrix P (defined in Hirsch, 1990), with the Jacobian A satisfying

$$A = P\Lambda P^{-1}, \text{ resulting in } \partial Q/\partial t + A\,\partial Q/\partial x = 0. \tag{13}$$

Hence an upwind formulation can be obtained with the Jacobians

$$A^+ = P\Lambda^+ P^{-1} \quad \text{and} \quad A^- = P\Lambda^- P^{-1}, \text{ with: } A = A^+ + A^- \text{ and } |A| = A^+ - A^-. \tag{14}$$

The fluxes associated with these split Jacobians are obtained from the remarkable property of homogeneity of the flux vector *f(Q)*. *f(Q)* is a homogeneous function of degree one of *Q*. Hence, *f = AQ* and the following flux splitting can be defined:

$$f^+ = A^+ Q \quad \text{and} \quad f^- = A^- Q, \text{ with: } f = f^+ + f^-. \tag{15}$$

This flux vector splitting, based on Eq. (9), has been introduced by Steger and Warming (1981). The split fluxes f^+ and f^- are also homogeneous functions of degree one in *Q*.

4.2 Arbitrary meshes

In practical computations one deal mostly with arbitrary meshes, considering either in a finite volume approach or in a curvilinear coordinate system.

In both cases, the upwind characterization is based on the signs of the eigenvalues of the matrix

$$K^{(n)} = \vec{A} \bullet \vec{n} = An_x + Bn_y + Cn_z, \tag{16}$$

where *A*, *B* and *C* are the Jacobian matrices written to the Cartesian system.

The fluxes will be decomposed by their components

$$\widetilde{F}^{(n)} = \vec{\vec{F}} \bullet \vec{n} = En_x + Fn_y + Gn_z \tag{17}$$

and separated into positive and negative parts according to the sign of the eigenvalues of $K^{(n)}$ as described above, considering the normal direction as a local coordinate direction.

For a general eigenvalue splitting, as Eq. (9), the normal flux projection, Eq. (17), is decomposed by a Steger and Warming (1981) flux splitting as

$$\widetilde{F}_{\pm}^{(n)} = \frac{\rho}{2\gamma} \left\{ \begin{array}{c} \alpha \\ \alpha u + a\left(\lambda_2^{\pm} - \lambda_3^{\pm}\right)n_x \\ \alpha v + a\left(\lambda_2^{\pm} - \lambda_3^{\pm}\right)n_y \\ \alpha w + a\left(\lambda_2^{\pm} - \lambda_3^{\pm}\right)n_z \\ \alpha \dfrac{u^2 + v^2 + w^2}{2} + av_n\left(\lambda_2^{\pm} - \lambda_3^{\pm}\right) + a^2 \dfrac{\lambda_2^{\pm} + \lambda_3^{\pm}}{\gamma - 1} \end{array} \right\}, \tag{18}$$

where the eigenvalues of the matrix K are defined as

$$\lambda_1 = \vec{v} \bullet \vec{n} \equiv v_n, \ \lambda_2 = \vec{v} \bullet \vec{n} + a \quad \text{and} \quad \lambda_3 = \vec{v} \bullet \vec{n} - a, \tag{19}$$

with $\vec{v}$ being the flow velocity vector, and $\pm$ sign indicates the positive or negative parts respectively. The parameter α is defined as

$$\alpha = 2(\gamma - 1)\lambda_1^{\pm} + \lambda_2^{\pm} + \lambda_3^{\pm}. \tag{20}$$

4.3 Definition of the RHS

The numerical scheme of Steger and Warming (1981) implemented in this work is based on a finite volume formulation, where the fluxes at interface are calculated as

$$\widetilde{F}_{i,j-1/2,k} = \left(\widetilde{F}_{i,j-1,k}^{-} + \widetilde{F}_{i,j,k}^{+}\right)S_{i,j-1/2,k}, \ \widetilde{F}_{i+1/2,j,k} = \left(\widetilde{F}_{i+1,j,k}^{-} + \widetilde{F}_{i,j,k}^{+}\right)S_{i+1/2,j,k}; \tag{21}$$

$$\widetilde{F}_{i,j+1/2,k} = \left(\widetilde{F}_{i,j+1,k}^{-} + \widetilde{F}_{i,j,k}^{+}\right)S_{i,j+1/2,k}, \ \widetilde{F}_{i-1/2,j,k} = \left(\widetilde{F}_{i-1,j,k}^{-} + \widetilde{F}_{i,j,k}^{+}\right)S_{i-1/2,j,k}; \tag{22}$$

$$\widetilde{F}_{i,j,k-1/2} = \left(\widetilde{F}_{i,j,k-1}^{-} + \widetilde{F}_{i,j,k}^{+}\right)S_{i,j,k-1/2}, \ \widetilde{F}_{i,j,k+1/2} = \left(\widetilde{F}_{i,j,k+1}^{-} + \widetilde{F}_{i,j,k}^{+}\right)S_{i,j,k+1/2}, \tag{23}$$

where S is the flux area calculated at each interface according to the procedure described in Section 3.

The Right-Hand-Side (RHS) of the Steger and Warming (1981) scheme, necessaries to the resolution of the implicit scheme, is defined by:

$$RHS(\ SW\ )_{i,j,k}^n = -\Delta t_{i,j,k} \Big/ V_{i,j,k} \left(\widetilde{F}_{i,j-1/2,k}^n + \widetilde{F}_{i+1/2,j,k}^n + \widetilde{F}_{i,j+1/2,k}^n + \widetilde{F}_{i-1/2,j,k}^n + \widetilde{F}_{i,j,k-1/2}^n + \widetilde{F}_{i,j,k+1/2}^n\right). \tag{24}$$

The terms in brackets at the RHS are a sum of normal fluxes because the correct signal of these fluxes is considered in Eqs. (21) to (23) by the signal of the normal unity vector components.

This version of the flux vector splitting algorithm of Steger and Warming (1981) is first order accurate in space. The second order version, with TVD properties, is implemented via a

MUSCL procedure (details in Hirsch, 1990). In this work, the non-linear limiter employed in the numerical simulations was the Minmod.

5 NUMERICAL SCHEME OF VAN LEER (1982)

The approximation to the integral Equation (1) to a hexahedron finite volume yields an ordinary differential equation system with respect to time:

$$V_{i,j,k} \, dQ_{i,j,k} \big/ dt = -R_{i,j,k} \,, \tag{25}$$

with $R_{i,j,k}$ representing the neat flux (residual) of the conservation of mass, of linear momentum and of energy in the $V_{i,j,k}$ volume. The residual is calculated as:

$$R_{i,j,k} = R_{i+1/2,j,k} - R_{i-1/2,j,k} + R_{i,j+1/2,k} - R_{i,j-1/2,k} + R_{i,j,k+1/2} - R_{i,j,k-1/2}\,, \tag{26}$$

where $R_{i+1/2,j,k} = R^c_{i+1/2,j,k}$, in which "c" is related to the flow convective contribution.

The discrete convective flux calculated by the AUSM scheme ("Advection Upstream Splitting Method") can be interpreted as a sum involving the arithmetical average between the right (R) and the left (L) states of the *(i+½,j,k)* cell face, related to cells *(i,j,k)* and *(i+1,j,k)*, respectively, multiplied by the interface Mach number, and a scalar dissipative term, as shown in Liou and Steffen Jr. (1993). Hence,

$$R_{i+1/2,j,k} = \left| S \right|_{i+1/2,j,k} \left(\frac{1}{2} M_{i+1/2,j,k} \left(\begin{bmatrix} \rho a \\ \rho a u \\ \rho a v \\ \rho a w \\ \rho a H \end{bmatrix}_L + \begin{bmatrix} \rho a \\ \rho a u \\ \rho a v \\ \rho a w \\ \rho a H \end{bmatrix}_R \right) - \frac{1}{2} \phi_{i+1/2,j,k} \left(\begin{bmatrix} \rho a \\ \rho a u \\ \rho a v \\ \rho a w \\ \rho a H \end{bmatrix}_R - \begin{bmatrix} \rho a \\ \rho a u \\ \rho a v \\ \rho a w \\ \rho a H \end{bmatrix}_L \right) \right) + \begin{bmatrix} 0 \\ S_x p \\ S_y p \\ S_z p \\ 0 \end{bmatrix}_{i+1/2,j,k} \,, \tag{27}$$

where $S_{i+1/2,j,k} = \begin{bmatrix} S_x & S_y & S_z \end{bmatrix}^T_{i+1/2,j,k}$ defines the normal area vector to the *(i+½,j,k)* surface.

The "*a*" quantity represents the speed of sound, calculated as $a = \sqrt{\gamma p / \rho}$. $M_{i+½,j,k}$ defines the advective Mach number at the *(i+½,j,k)* face of the cell *(i,j,k)*, which is calculated according to Liou and Steffen Jr. (1993) as:

$$M_{i+1/2,j,k} = M^+_L + M^-_R \,, \tag{28}$$

where the $M^{+/-}$ separated Mach numbers are defined by Van Leer (1982) as:

$$M^+ = \begin{bmatrix} M, & if \ M \ge 1; \\ 0.25(M+1)^2, & if \ |M| < 1; \\ 0, & if \ M \le -1; \end{bmatrix} \quad and \quad M^- = \begin{bmatrix} 0, & if \ M \ge 1; \\ -0.25(M-1)^2, & if \ |M| < 1; \\ M, & if \ M \le -1. \end{bmatrix} \tag{29}$$

M_L and M_R represent the Mach numbers associated to the left and right states, respectively. The advection Mach number is defined as:

$$M = \left(S_x u + S_y v + S_z w\right) / \left(a|S|\right).$$ (30)

The pressure at the *(i+½,j,k)* face of the *(i,j,k)* cell is calculated from a similar way:

$$p_{i+1/2,j,k} = p_L^+ + p_R^-,$$ (31)

with $p^{+/-}$ representing the pressure separation defined according to Van Leer (1982):

$$p^+ = \begin{bmatrix} p, & if\ M \geq 1; \\ 0.25p(M+1)^2(2-M), & if\ |M| < 1; \\ 0, & if\ M \leq -1; \end{bmatrix} \text{ and } p^- = \begin{bmatrix} 0, & if\ M \geq 1; \\ 0.25p(M-1)^2(2+M), & if\ |M| < 1; \\ p, & if\ M \leq -1. \end{bmatrix}$$ (32)

The definition of the ϕ dissipation term determines the particular formulation to the convective fluxes. The following choice corresponds to the Van Leer (1982) scheme, according to Radespiel and Kroll (1995):

$$\phi_{i+1/2,j,k} = \phi_{i+1/2,j,k}^{VL} = \begin{pmatrix} \left|M_{i+1/2,j,k}\right|, & if\ \left|M_{i+1/2,j,k}\right| \geq 1; \\ \left|M_{i+1/2,j,k}\right| + 0.5(M_R - 1)^2, & if\ 0 \leq M_{i+1/2,j,k} < 1; \\ \left|M_{i+1/2,j,k}\right| + 0.5(M_L + 1)^2, & if\ -1 < M_{i+1/2,j,k} \leq 0. \end{pmatrix}$$ (33)

The right-hand-side of the Van Leer (1982) scheme, necessaries to the implicit resolution of this algorithm, is defined as:

$$RHS(VL)_{i,j,k}^n = -\Delta t_{i,j,k} / V_{i,j,k} \left(R_{i+1/2,j,k}^n - R_{i-1/2,j,k}^n + R_{i,j+1/2,k}^n - R_{i,j-1/2,k}^n + R_{i,j,k+1/2}^n - R_{i,j,k-1/2}^n\right).$$ (34)

The terms in brackets at the RHS are a sum of differences of normal fluxes because the correct signal of these fluxes is not completely considered in Eq. (27), requiring that the correct signal should be considered explicitly.

This version of the Van Leer (1982) scheme is first order accurate in space. The second order version, with TVD properties, is implemented via a MUSCL procedure (details in Hirsch, 1990). In this work, the non-linear limiter employed in the numerical simulations was the Minmod.

6 IMPLICIT FORMULATION

Both implicit schemes implemented in this work used backward Euler in time and ADI approximate factorization to solve a three-diagonal system in each direction.

The ADI approximate factorization form to the implicit schemes of Steger and Warming (1981) and of Van Leer (1982) is presented in three stages, each one associated with a different coordinate direction:

$$\left[I + \Delta t_{i,j,k} \Delta_+^\xi A_{i+1/2,j,k}^- + \Delta t_{i,j,k} \Delta_-^\xi A_{i+1/2,j,k}^+\right] \Delta Q_{i,j,k}^* = RHS_{i,j,k};$$ (35)

$$\left[I + \Delta t_{i,j,k} \Delta_+^\eta B_{i,j+1/2,k}^- + \Delta t_{i,j,k} \Delta_-^\eta B_{i,j+1/2,k}^+\right] \Delta Q_{i,j,k}^{**} = \Delta Q_{i,j,k}^*;$$ (36)

$$\left[I + \Delta t_{i,j,k} \Delta_+^\zeta C_{i,j+1/2,k}^- + \Delta t_{i,j,k} \Delta_-^\zeta C_{i,j+1/2,k}^+\right] \Delta Q_{i,j,k}^{n+1} = \Delta Q_{i,j,k}^{**},$$ (37)

where: $RHS_{i,j,k}$ is defined by Eqs. (24) or (34), depending if the Steger and Warming (1981) or the Van Leer (1982) scheme is being solved, respectively; the difference operators are defined as:

$$\Delta_+^\xi(\cdot) = (\cdot)_{i+1,j,k} - (\cdot)_{i,j,k}\,, \ \ \Delta_-^\xi(\cdot) = (\cdot)_{i,j,k} - (\cdot)_{i-1,j,k}\,, \ \ \Delta_+^\eta(\cdot) = (\cdot)_{i,j+1,k} - (\cdot)_{i,j,k}\,; \tag{38}$$

$$\Delta_-^\eta(\cdot) = (\cdot)_{i,j,k} - (\cdot)_{i,j-1,k}\,, \ \ \Delta_+^\zeta(\cdot) = (\cdot)_{i,j,k+1} - (\cdot)_{i,j,k}\,, \ \ \Delta_-^\zeta(\cdot) = (\cdot)_{i,j,k} - (\cdot)_{i,j,k-1}\,. \tag{39}$$

and the update of the conserved variable vector is proceeded as follows:

$$Q_{i,j,k}^{n+1} = Q_{i,j,k}^n + \Delta Q_{i,j,k}^{n+1}\,. \tag{40}$$

This system of 5x5 block three-diagonal linear equations is solved using LU decomposition and the Thomas algorithm applied to systems of block matrices.

The splitting matrices A^+, A^-, B^+, B^-, C^+ and C^- are defined as:

$$A^+ = T_\xi \Lambda_\xi^+ T_\xi^{-1}\,, \ \ A^- = T_\xi \Lambda_\xi^- T_\xi^{-1}\,, \ \ B^+ = T_\eta \Lambda_\eta^+ T_\eta^{-1}\,, \ \ B^- = T_\eta \Lambda_\eta^- T_\eta^{-1}\,, \ \ C^+ = T_\zeta \Lambda_\zeta^+ T_\zeta^{-1}\,; \tag{41}$$

$$C^- = T_\zeta \Lambda_\zeta^- T_\zeta^{-1}\,, \tag{42}$$

where the similar transformation matrix T and its inverse specified by:

$$[T] = \begin{bmatrix} h_x' & h_y' & h_z' \\ h_x' u_{int} & h_y' u_{int} - h_z' \rho_{int} & h_z' u_{int} - h_y' \rho_{int} \\ h_x' v_{int} + h_z' \rho_{int} & h_y' v_{int} & h_z' v_{int} - h_x' \rho_{int} \\ h_x' w_{int} - h_y' \rho_{int} & h_y' w_{int} + h_x' \rho_{int} & h_z' w_{int} \\ h_x' \phi^2/(\gamma-1) + \rho_{int}\left(h_z' v_{int} - h_y' w_{int}\right) & h_y' \phi^2/(\gamma-1) + \rho_{int}\left(h_x' w_{int} - h_z' u_{int}\right) & h_z' \phi^2/(\gamma-1) + \rho_{int}\left(h_y' u_{int} - h_x' v_{int}\right) \end{bmatrix}$$

$$\begin{matrix} \alpha & \alpha \\ \alpha\left(u_{int} + h_x' a_{int}\right) & \alpha\left(u_{int} - h_x' a_{int}\right) \\ \alpha\left(v_{int} + h_y' a_{int}\right) & \alpha\left(v_{int} - h_y' a_{int}\right) \\ \alpha\left(w_{int} + h_z' a_{int}\right) & \alpha\left(w_{int} - h_z' a_{int}\right) \\ \alpha\left[\left(\phi^2 + a_{int}^2\right)/(\gamma-1) + a_{int}\tilde{\theta}\right] & \alpha\left[\left(\phi^2 + a_{int}^2\right)/(\gamma-1) - a_{int}\tilde{\theta}\right] \end{matrix}\,, \tag{43}$$

$$[T^{-1}] = \begin{bmatrix} h_x'\left(1 - \phi^2/a_{int}^2\right) - \left(h_z' v_{int} - h_y' w_{int}\right)/\rho_{int} & h_x'(\gamma-1)u_{int}/a_{int}^2 & h_z'/\rho_{int} + h_x'(\gamma-1)v_{int}/a_{int}^2 \\ h_y'\left(1 - \phi^2/a_{int}^2\right) - \left(h_x' w_{int} - h_z' u_{int}\right)/\rho_{int} & -h_z'/\rho_{int} + h_y'(\gamma-1)u_{int}/a_{int}^2 & h_y'(\gamma-1)v_{int}/a_{int}^2 \\ h_z'\left(1 - \phi^2/a_{int}^2\right) - \left(h_y' u_{int} - h_x' v_{int}\right)/\rho_{int} & h_y'/\rho_{int} + h_z'(\gamma-1)u_{int}/a_{int}^2 & -h_x'/\rho_{int} + h_z'(\gamma-1)v_{int}/a_{int}^2 \\ \beta\left(\phi^2 - a_{int}\tilde{\theta}\right) & \beta\left[h_x' a_{int} - (\gamma-1)u_{int}\right] & \beta\left[h_y' a_{int} - (\gamma-1)v_{int}\right] \\ \beta\left(\phi^2 + a_{int}\tilde{\theta}\right) & -\beta\left[h_x' a_{int} - (\gamma-1)u_{int}\right] & -\beta\left[h_y' a_{int} - (\gamma-1)v_{int}\right] \end{bmatrix}$$

$$\begin{matrix} -h_y'/\rho_{int} + h_x'(\gamma-1)w_{int}/a_{int}^2 & -h_x'(\gamma-1)/a_{int}^2 \\ h_x'/\rho_{int} + h_y'(\gamma-1)w_{int}/a_{int}^2 & -h_y'(\gamma-1)/a_{int}^2 \\ h_z'(\gamma-1)w_{int}/a_{int}^2 & -h_z'(\gamma-1)/a_{int}^2 \\ \beta\left[h_z' a_{int} - (\gamma-1)w_{int}\right] & \beta(\gamma-1) \\ -\beta\left[h_z' a_{int} + (\gamma-1)w_{int}\right] & \beta(\gamma-1) \end{matrix}\,, \tag{44}$$

with the general parameters defined according to:

$$\alpha = \rho_{int} / \left(\sqrt{2} a_{int} \right), \ \beta = 1 / \left(\sqrt{2} \rho_{int} a_{int} \right), \ \phi^2 = 0.5(\gamma - 1)\left(u_{int}^2 + v_{int}^2 + w_{int}^2 \right) \tag{45}$$

and the specific parameter defined by:

$$\tilde{\theta} = h_x' u_{int} + h_y' v_{int} + h_z' w_{int}, \tag{46}$$

with the metric terms to this generalized coordinate system defined as:

$$h_x = S_{x\_int} / V_{int} \ , \ h_y = S_{y\_int} / V_{int} \ , \ h_z = S_{z\_int} / V_{int} \quad \text{and} \quad h_n = S / V_{int} \ , \tag{47}$$

where $S_{x\_int} = n_x S$, $S_{y\_int} = n_y S$, $S_{z\_int} = n_z S$ are de Cartesian components of the flux area and S is the flux area, calculated as described in section 3. The V_{int} is calculated as the arithmetical average between the volumes which shares the flux interface. The normalized metric terms are given by:

$$h_x' = h_x / h_n \ , \ h_y' = h_y / h_n \quad \text{and} \quad h_z' = h_z / h_n \ . \tag{48}$$

The interface values are obtained by arithmetical average between right and left states of the interface flux face. Finally, the diagonal matrices of eigenvalues are determined by:

$$\Lambda_\xi^+ = \begin{bmatrix} \lambda_1^{\xi,+} & & & & \\ & \lambda_2^{\xi,+} & & & \\ & & \lambda_3^{\xi,+} & & \\ & & & \lambda_4^{\xi,+} & \\ & & & & \lambda_5^{\xi,+} \end{bmatrix} \quad \text{and} \quad \Lambda_\xi^- = \begin{bmatrix} \lambda_1^{\xi,-} & & & & \\ & \lambda_2^{\xi,-} & & & \\ & & \lambda_3^{\xi,-} & & \\ & & & \lambda_4^{\xi,-} & \\ & & & & \lambda_5^{\xi,-} \end{bmatrix} ; \tag{49}$$

$$\Lambda_\eta^+ = \begin{bmatrix} \lambda_1^{\eta,+} & & & & \\ & \lambda_2^{\eta,+} & & & \\ & & \lambda_3^{\eta,+} & & \\ & & & \lambda_4^{\eta,+} & \\ & & & & \lambda_5^{\eta,+} \end{bmatrix} \quad \text{and} \quad \Lambda_\eta^- = \begin{bmatrix} \lambda_1^{\eta,-} & & & & \\ & \lambda_2^{\eta,-} & & & \\ & & \lambda_3^{\eta,-} & & \\ & & & \lambda_4^{\eta,-} & \\ & & & & \lambda_5^{\eta,-} \end{bmatrix} ; \tag{50}$$

$$\Lambda_\zeta^+ = \begin{bmatrix} \lambda_1^{\zeta,+} & & & & \\ & \lambda_2^{\zeta,+} & & & \\ & & \lambda_3^{\zeta,+} & & \\ & & & \lambda_4^{\zeta,+} & \\ & & & & \lambda_5^{\zeta,+} \end{bmatrix} \quad \text{and} \quad \Lambda_\zeta^- = \begin{bmatrix} \lambda_1^{\zeta,-} & & & & \\ & \lambda_2^{\zeta,-} & & & \\ & & \lambda_3^{\zeta,-} & & \\ & & & \lambda_4^{\zeta,-} & \\ & & & & \lambda_5^{\zeta,-} \end{bmatrix} , \tag{51}$$

with the eigenvalues of the Euler equations in the ξ, η and ζ directions, normal to the respective cell faces, evaluated by:

$$v_n = u_{int} h_x + v_{int} h_y + w_{int} h_z \ , \ \lambda_1 = v_n \ , \ \lambda_2 = v_n \ , \ \lambda_3 = v_n \ , \ \lambda_4 = v_n + a_{int} h_n \ , \ \lambda_5 = v_n - a_{int} h_n \ , \tag{52}$$

where the eigenvalue splitting defined according to Steger and Warming (1981), Eq. (9). This implicit formulation to the Left-Hand-Side (LHS) of the Steger and Warming (1981) and of the Van Leer (1982) schemes is first order accurate in time and space. As the steady state condition is the desirable solution, the spatial solution accuracy is determined by the RHS accuracy, which is second order with the MUSCL implementation on both schemes, since the LHS tends to zero in the steady condition.

7 SPATIALLY VARIABLE TIME STEP

The idea of a spatially variable time step consists in keeping constant a CFL number in the calculation domain and to guarantee time steps appropriated to each mesh region during the convergence process. The spatially variable time step can be defined by:

$$\Delta t_{i,j,k} = \frac{CFL(\Delta s)_{i,j,k}}{(|q|+a)_{i,j,k}},\tag{53}$$

where CFL is the Courant-Friedrichs-Lewis number to method stability; $(\Delta s)_{i,j,k}$ is a characteristic length of information transport; and $(|q|+a)_{i,j,k}$ is the maximum characteristic speed of information transport, where a is the speed of sound. The characteristic length of information transport, $(\Delta s)_{i,j,k}$, can be determined by:

$$(\Delta s)_{i,j,k} = \left[MIN(l_{MIN}, C_{MIN}) \right]_{i,j,k},\tag{54}$$

where l_{MIN} is the minimum side length which forms a computational cell and C_{MIN} is the minimum distance of baricenters among the computational cell and its neighbors. The maximum characteristic speed of information transport is defined by $(|q|+a)_{i,j,k}$, with $q = \sqrt{u^2 + v^2 + w^2}$.

8 INITIAL AND BOUNDARY CONDITIONS

8.1 Initial condition

The initial condition adopted for the problems is the freestream flow in all calculation domain (Jameson and Mavriplis, 1986, and Maciel, 2002). The vector of conserved variables is expressed as follows:

$$Q_\infty = \left\{ 1 \quad M_\infty \cos\theta \quad M_\infty sen\theta \cos\psi \quad M_\infty sen\theta sen\psi \quad \left[\frac{1}{\gamma(\gamma-1)} + \frac{M_\infty^2}{2} \right] \right\}^t,\tag{55}$$

where M_∞ represents the freestream Mach number, θ is the flow incidence angle downstream the configuration under study and ψ is the angle in the configuration longitudinal plane.

8.2 Boundary conditions

The different types of implemented boundary conditions are described as follows. They are implemented in special cells named "ghost cells", as referred in the Computational Fluid Dynamics (CFD) community.

a) Wall - The Euler case requires the flux tangency condition. On the context of finite volumes, this imposition is done considering that the tangent flow velocity component to the wall of the ghost cell be equal to the tangent flow velocity component to the wall of the neighbor real cell. At the same time, the normal flow velocity component to the wall of the ghost cell should be equal to the negative of the normal flow velocity component to the wall of the neighbor real cell. Batina (1993) suggests that these procedures lead to the following expressions to the velocity components *u*, *v* and *w* of the ghost cells:

$$u_g = (1 - 2n_x n_x)u_{real} + (-2n_x n_y)v_{real} + (-2n_x n_z)w_{real} ; \qquad (56)$$

$$v_g = (-2n_y n_x)u_{real} + (1 - 2n_y n_y)v_{real} + (-2n_y n_z)w_{real} ; \qquad (57)$$

$$w_g = (-2n_z n_x)u_{real} + (-2n_z n_y)v_{real} + (1 - 2n_z n_z)w_{real} . \qquad (58)$$

The fluid pressure gradient in the direction normal to the wall is equal to zero for the inviscid case. The temperature gradient is equal to zero along the whole wall, according to the condition of adiabatic wall. With these two conditions, a zero order extrapolation is performed to the fluid pressure and to the temperature. It is possible to conclude that the fluid density will also be obtained by zero order extrapolation. The energy conserved variable is obtained from the state equation to a perfect gas, Eq. (3).

b) Far field - In the implementation of the boundary conditions in the mesh limit external region to the ramp problem (external flow), it is necessary to identify four possible situations: entrance with subsonic flow, entrance with supersonic flow, exit with subsonic flow and exit with supersonic flow. These situations are described below.

b.1) Entrance with subsonic flow – Considering the one-dimensional characteristic relation concept in the normal direction of flow penetration, the entrance with subsonic flow presents four characteristic velocities of information propagation which have direction and orientation point inward the calculation domain, which implies that the variables associated with these waves cannot be extrapolated (Maciel, 2002). It is necessary to specify four conditions to these four information. Jameson and Mavriplis (1986) indicate as appropriated quantities to be specified the freestream density and the freestream Cartesian velocity components *u*, *v* and *w*. Just the last characteristics, "*(q_n-a)*", which transports information from inside to outside of the calculation domain, cannot be specified and will have to be determined by interior information of the calculation domain. In this work, a zero order extrapolation to the pressure is performed, being the total energy defined by the state equation of a perfect gas.

b.2) Entrance with supersonic flow - All variables are specified at the entrance boundary, adopting freestream values.

b.3) Exit with subsonic flow - Four characteristics which govern the Euler equations proceed from the internal region of the calculation domain. So, the density and the Cartesian velocity components are extrapolated from the interior domain (Maciel, 2002). One condition should be specified to the boundary. In this case, the pressure is fixed in the calculation domain exit, keeping its respective value of freestream flow. Total energy is specified by the equation of state to a perfect gas.

b.4) Exit with supersonic flow - The five characteristics which govern the Euler equations proceed from the internal region of the calculation domain. It is not possible to specify variable values at the exit. The zero order extrapolation is applied to density, Cartesian

velocity components and pressure. Total energy is specified by the equation of state to a perfect gas.

c)   Entrance and exit – The entrance and exit boundaries are applied to the ramp and diffuser problems. Boundary conditions which involve flow entrance in the calculation domain had the flow properties fixed with freestream values. Boundary conditions which involve flow exit of the computational domain used simply the zero order extrapolation to the determination of properties in this boundary. This procedure is correct because the entrance flow and the exit flow are no minimal supersonic to both studied examples.

9   RESULTS

Tests were performed in a microcomputer with processor AMD SEMPRON (tm) 2600+, 1.83GHz, and 512 Mbytes of RAM. As the interest of this work is steady state problems, one needs to define a criterion which guarantees that such condition was reached. The criterion adopted in this work was to consider a reduction of 3 orders in the magnitude of the maximum residual in the domain, a typical criterion in the CFD community. The residual to each cell was defined as the numerical value obtained from the discretized conservation equations. As there are five conservation equations to each cell, the maximum value obtained from these equations is defined as the residual of this cell. Thus, this residual is compared with the residual of the others cells, calculated of the same way, to define the maximum residual in the domain. The configuration downstream and the configuration longitudinal plane angles were set equal to 0.0°.

The physical problems to be studied are the supersonic flow along a ramp with 20° of inclination and the "cold gas" hypersonic flow along a diffuser also with 20° of inclination at the contraction region. The ramp and diffuser configurations in the xy plane are described in Figs. 6 and 7. The ramp spanwise length is 0.25m, while the diffuser spanwise length is 0.10m.
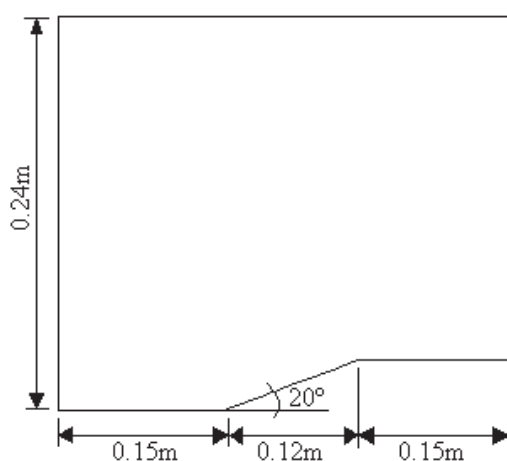
Figure 6: Ramp configuration in the xy plane.
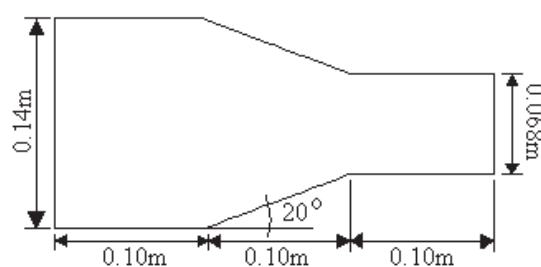
Figure 7: Diffuser configuration in the xy plane.

	Ramp	Diffuser
Finite difference representation	61(ξ)x60(η)x10(ζ)	61(ξ)x51(η)x10(ζ)
Cells (Finite Volumes)	31,860	27,000
Nodes (Finite volumes)	36,600	31,110

Table 1: Computational data of the ramp and diffuser meshes.

In the ramp problem, an oblique shock wave and an expansion fan are formed, at the ramp and after the ramp, respectively. In the diffuser problem, the two oblique shock waves originated by the convergent walls suffer interference after the throat and expansions waves are formed after the contraction region in both upper and lower walls.

The computational data of the generated meshes to both problems are presented in Tab. 1.

9.1 Ramp physical problem

The freestream Mach number adopted as initial condition to this simulation was 3.0, characterizing a supersonic flow regime.

Figures 8 to 11 show the density contours obtained by the Steger and Warming (1981) first order scheme, the Van Leer (1982) first order scheme, the Steger and Warming (1981) high resolution TVD scheme using Minmod limiter and the Van Leer (1982) high resolution TVD scheme using Minmod limiter, respectively. All solutions present good quality characteristics with the shock being well captured by all schemes. The Van Leer (1982) TVD scheme using Minmod limiter presents the densest field in comparison with the others schemes.
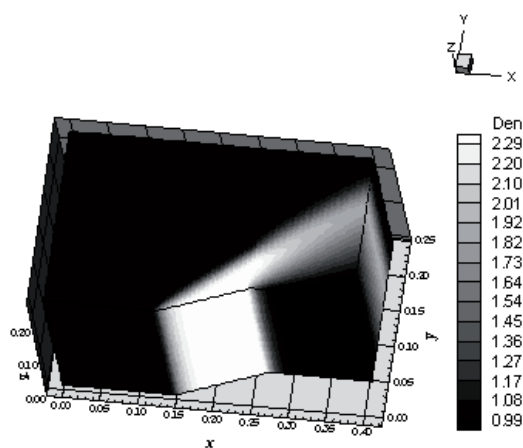
Figure 8: Density contours (SW-1a).
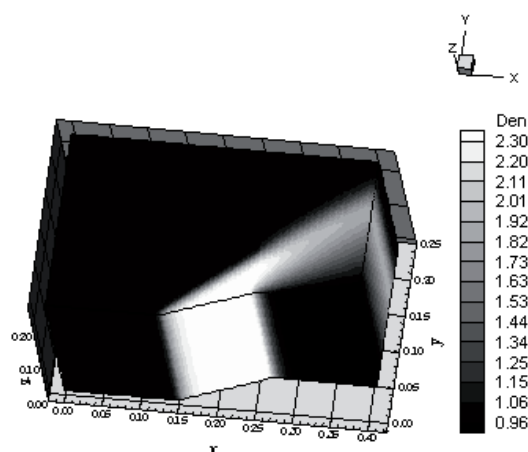
Figure 9: Density contours (VL-1a).
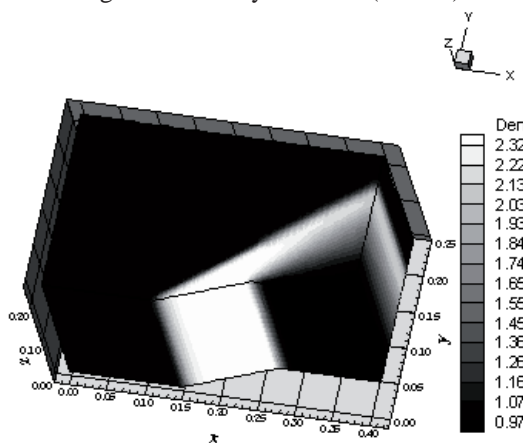
Figure 10: Density contours (SW-2a-MIN).
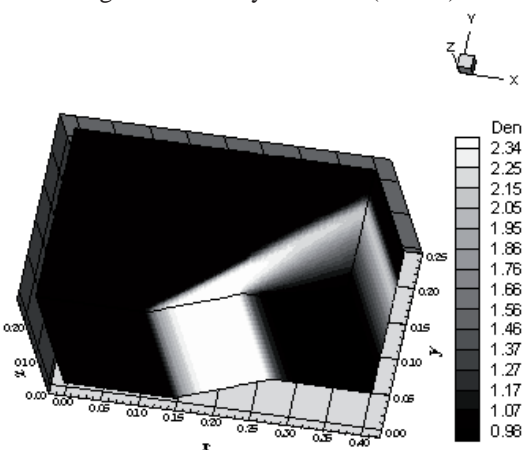
Figure 11: Density contours (VL-2a-MIN).

Figures 12 to 15 exhibit the pressure contours obtained by the Steger and Warming (1981) first order scheme, the Van Leer (1982) first order scheme, the Steger and Warming (1981) TVD scheme using Minmod limiter and the Van Leer (1982) TVD scheme using Minmod limiter, respectively. The most severe pressure field was obtained by the Steger and

Warming (1981) TVD scheme using Minmod limiter. Good qualitative characteristics are observed in all solutions with the oblique shock wave appropriately captured.
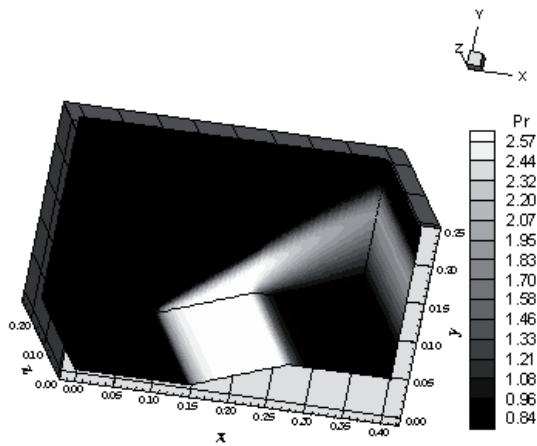
Figure 12: Pressure contours (SW-1a).
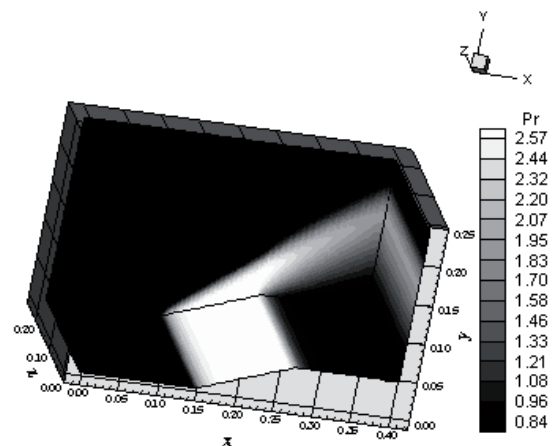
Figure 13: Pressure contours (VL-1a).
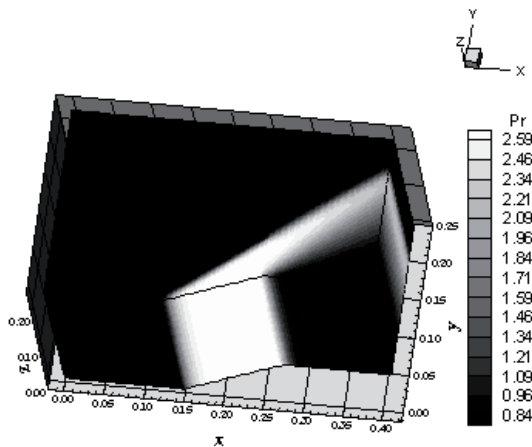
Figure 14: Pressure contours (SW-2a-MIN).
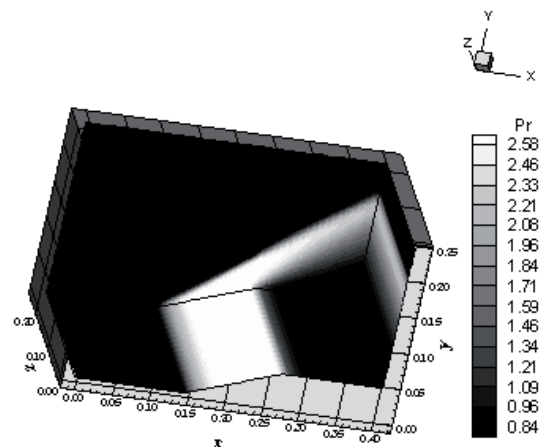
Figure 15: Pressure contours (VL-2a-MIN).
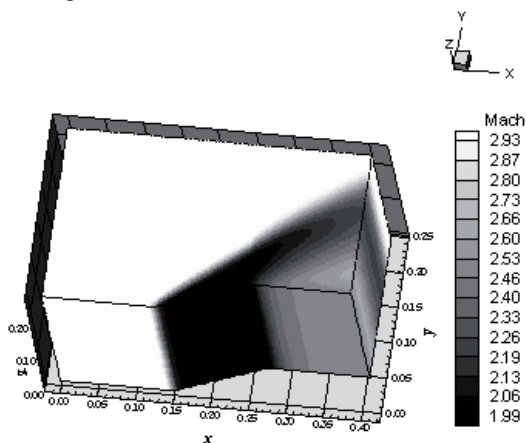
Figure 16: Mach contours (SW-1a).
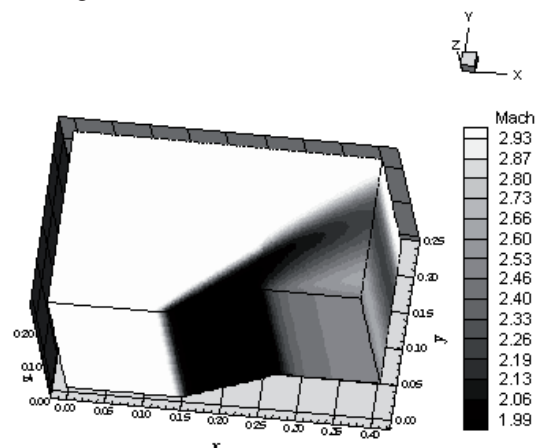
Figure 17: Mach contours (VL-1a).

Figures 16 to 19 show the Mach number contours obtained by the Steger and Warming (1981) first order scheme, the Van Leer (1982) first order scheme, the Steger and Warming (1981) TVD scheme using Minmod limiter and the Van Leer (1982) TVD scheme using Minmod limiter, respectively. The Van Leer (1982) TVD scheme using Minmod limiter presents the most intense Mach number field in comparison with the others schemes.
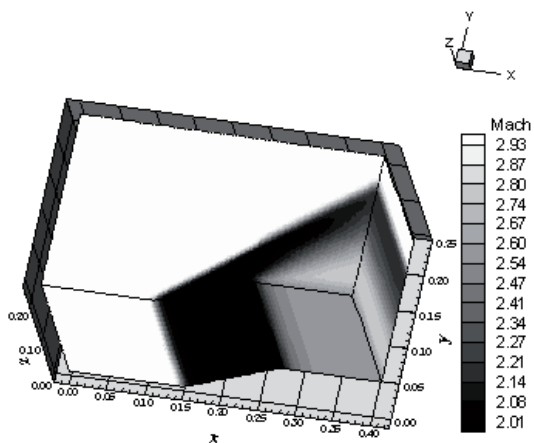
Figure 18: Mach contours (SW-2a-MIN).   Figure 19: Mach contours (VL-2a-MIN).
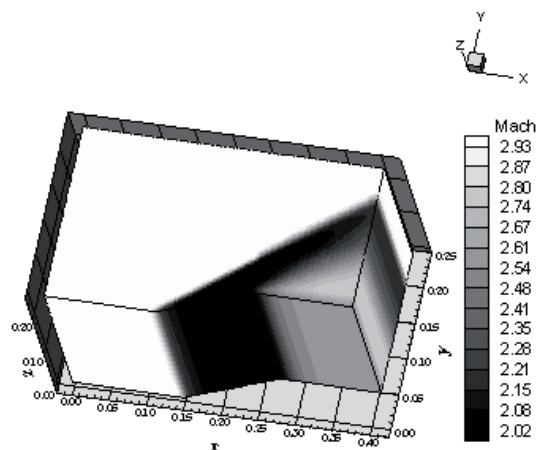
Figure 20 presents the wall pressure distributions obtained with the Steger and Warming (1981) TVD scheme using Minmod limiter and the Van Leer (1982) TVD scheme using Minmod limiter, evaluated at the computational plane k = kmax/2, where "kmax" is the maximum number of points at the z direction. They are compared with exact solutions of the oblique shock wave and the Prandtl-Meyer expansion theories. Both schemes represent accurately the pressure plateau at the ramp, agreeing with the oblique shock wave theory. However, the best width of the pressure plateau is determined by the Steger and Warming (1981) TVD scheme using Minmod limiter. Both schemes detect appropriately the pressure at the end of the expansion fan, after the ramp.
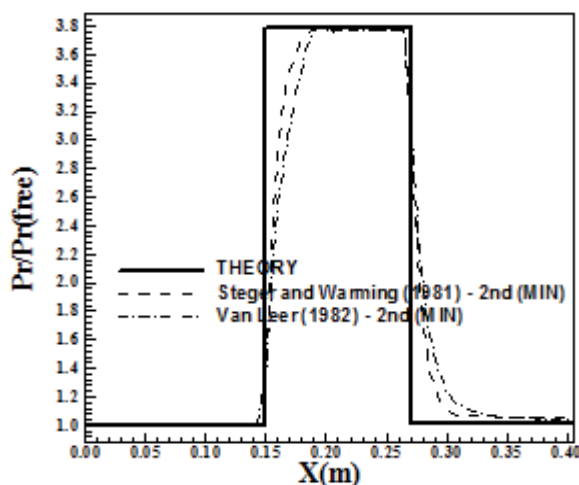
Figure 20: Wall pressure distributions.

Figure 21 exhibits the wall pressure distributions obtained only with the Steger and Warming (1981) versions, first order and TVD variant. They are again compared with exact solutions of the oblique shock wave and the Prandtl-Meyer expansion theories. As expected, the TVD variant presents better pressure width at the pressure plateau, appropriately estimation of the pressure at the ramp and better pressure at the end of the expansion fan. Figure 22 shows the wall pressure distributions obtained only with the Van Leer (1982) versions, first order and TVD variant. Opposed to the behavior observed with the Steger and Warming (1981) TVD scheme, the first order Van Leer (1982) scheme presents the best pressure width at the pressure plateau. However, the pressure at the ramp and the pressure at

the end of the expansion fan are better estimated by the TVD variant of the Van Leer (1982) scheme.
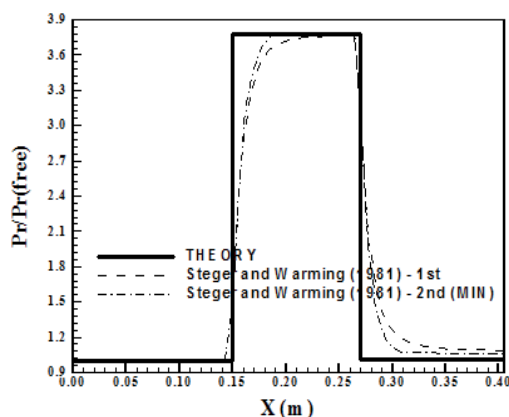
Figure 21: Wall pressure distributions (SW).
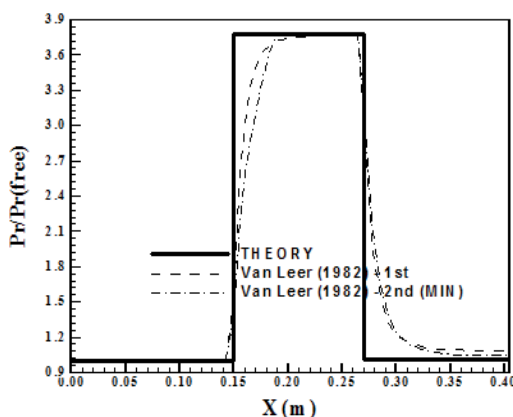
Figure 22: Wall pressure distributions (VL).

One way to quantitatively verify if the solutions generated by each scheme are satisfactory consists in determining the shock angle of the oblique shock wave, β, measured in relation to the initial direction of the flow field. Anderson Jr. (1984) (pages 352 and 353) presents a diagram with values of the shock angle, β, to oblique shock waves. The value of this angle is determined as function of the freestream Mach number and of the deflection angle of the flow after the shock wave, ϕ. To $\phi = 20º$ (ramp inclination angle) and to a freestream Mach number equals to 3.0, it is possible to obtain from this diagram a value to β equals to 37.7º. Using a transfer in Figures 12 to 15, considering the xy plane, it is possible to obtain the values of β to each scheme, as well the respective errors shown in Tab. 2. Basically, all schemes predicted accurately the shock angle of the oblique shock wave, with errors less than 1%. The exception is the first order scheme of Van Leer (1982).

Algorithm:	β (°)	Error (%)
Steger and Warming (1981) – 1a	38.0	0.796
Steger and Warming (1981) – 2a – Minmod	38.0	0.796
Van Leer (1982) – 1a	38.5	2.122
Van Leer (1982) – 2a – Minmod	37.4	0.796

Table 2: Shock angle of the oblique shock wave at the ramp and percentage error to each scheme.

9.2 Diffuser physical problem

The freestream Mach number adopted as initial condition to this simulation was 7.0, characterizing a "cold gas" hypersonic flow regime. Results with the Steger and Warming (1981) scheme, in its first order and second order versions, and the Van Leer (1982) scheme, also in its first order and second order versions, are presented.

Figures 23 to 26 show the density contours obtained by the Steger and Warming (1981) first order scheme, the Van Leer (1982) first order scheme, the Steger and Warming (1981) TVD scheme using Minmod limiter and the Van Leer (1982) TVD scheme using Minmod limiter, respectively. All solutions present good quality characteristics with the shock interference being well captured by all schemes. The Van Leer (1982) TVD scheme using Minmod limiter presents the densest field in comparison with the others schemes.

Figures 27 to 30 exhibit the pressure contours obtained by the Steger and Warming (1981) first order scheme, the Van Leer (1982) first order scheme, the Steger and Warming

(1981) TVD scheme using Minmod limiter and the Van Leer (1982) TVD scheme using Minmod limiter, respectively. The Van Leer (1982) TVD scheme using Minmod limiter presents the most severe pressure field in comparison with the others schemes.
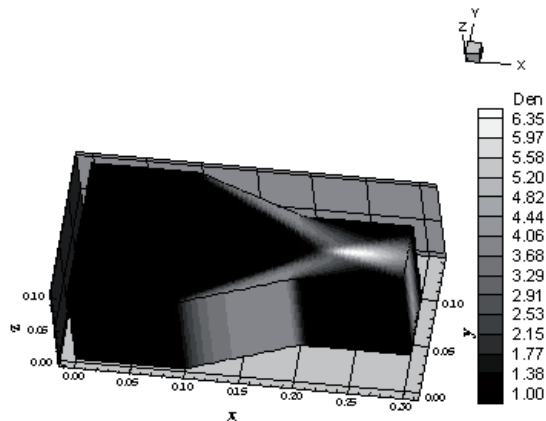
Figure 23: Density contours (SW-1a).
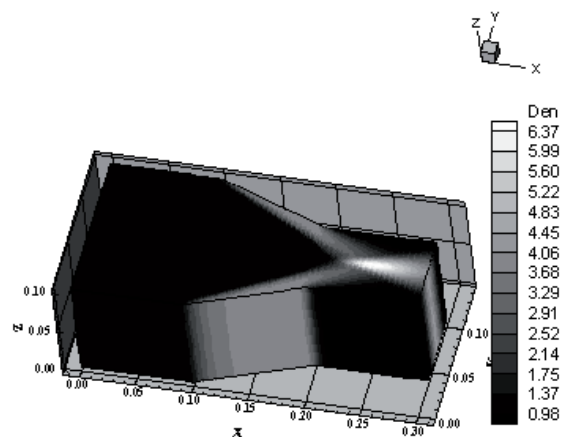
Figure 24: Density contours (VL-1a).
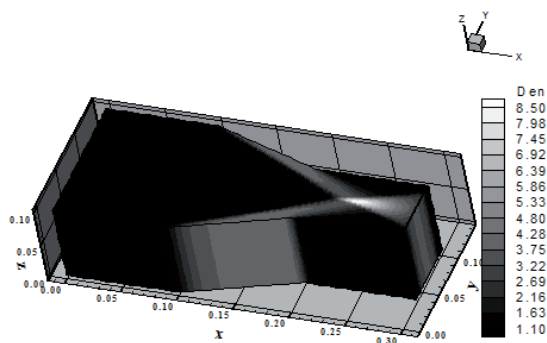
Figure 25: Density contours (SW-2a-MIN).
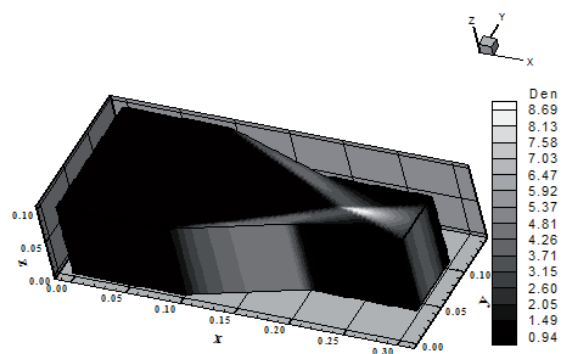
Figure 26: Density contours (VL-2a-MIN).
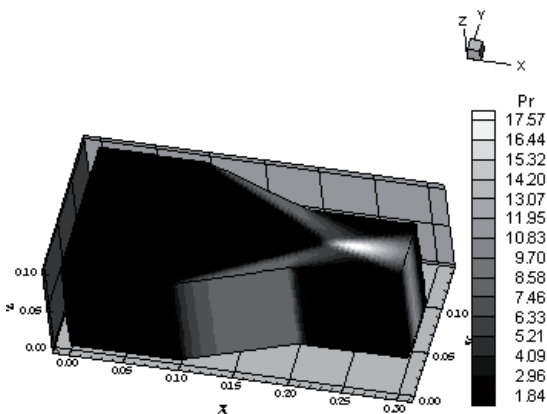
Figure 27: Pressure contours (SW-1a).
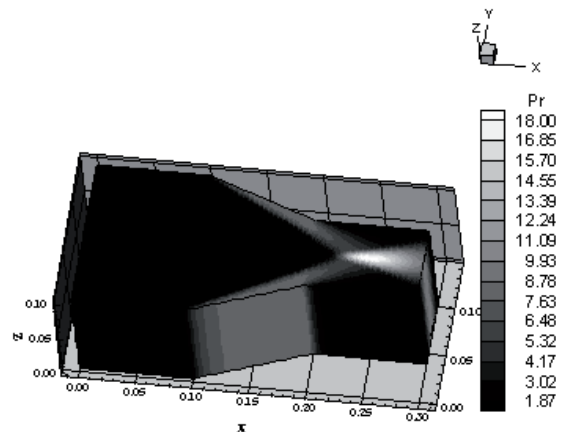
Figure 28: Pressure contours (VL-1a).

Figures 31 to 34 show the Mach number contours obtained by the Steger and Warming (1981) first order scheme, the Van Leer (1982) first order scheme, the Steger and Warming (1981) TVD scheme using Minmod limiter and the Van Leer (1982) TVD scheme using Minmod limiter, respectively. The first order scheme of Steger and Warming (1981) presents the most intense Mach number field.

Figure 35 exhibits the lower wall pressure distributions obtained only with the Steger and Warming (1981) versions, first order and TVD variant. They are again compared with exact solutions of the oblique shock wave and the Prandtl-Meyer expansion theories. As expected,

the TVD variant present better pressure width at the pressure plateau, underprediction of the pressure at the ramp (convergent region of the diffuser), also observed in the first order version, and better pressure at the end of the expansion fan. Figure 36 shows the lower wall pressure distributions obtained only with the Van Leer (1982) versions, first order and TVD variant. Again, opposed to the behavior observed with the Steger and Warming (1981) TVD scheme, the first order Van Leer (1982) scheme presents the best pressure width at the pressure plateau. The pressure at the ramp is underpredicted by all versions of the Van Leer (1982) scheme and the pressure at the end of the expansion fan is better estimated by the first order version of the Van Leer (1982) scheme.
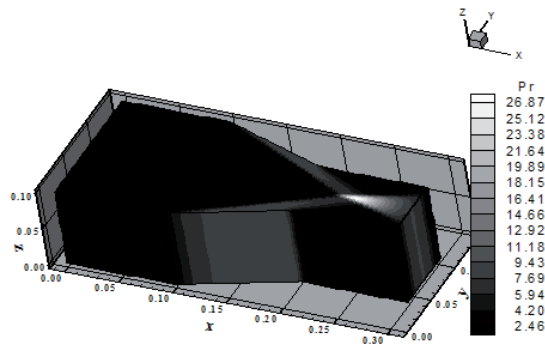
Figure 29: Pressure contours (SW-2a-MIN).
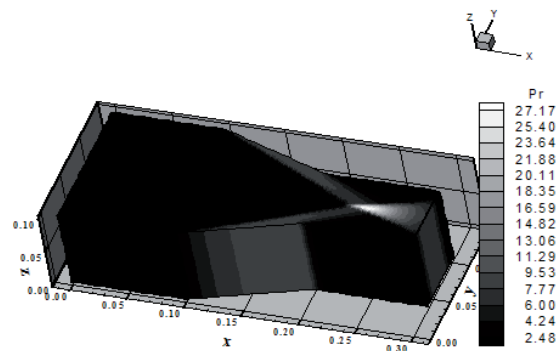
Figure 30: Pressure contours (VL-2a-MIN).
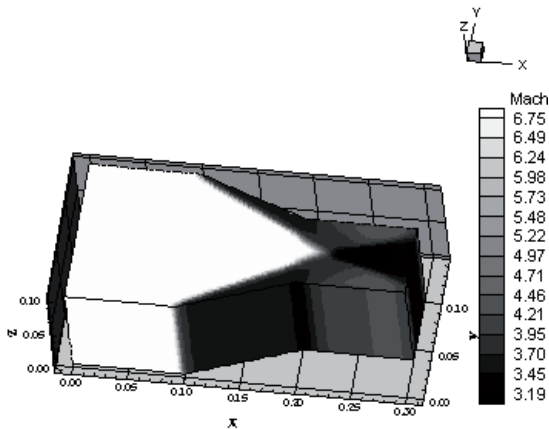
Figure 31: Mach contours (SW-1a).
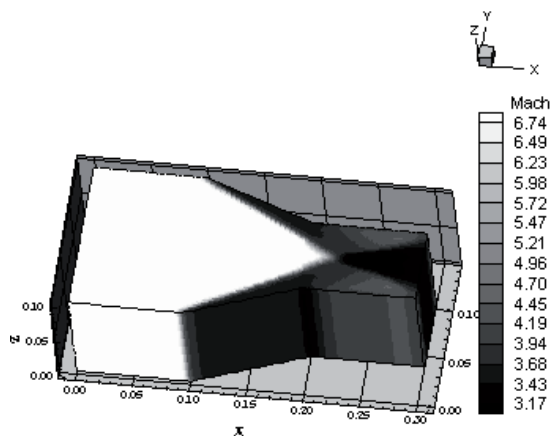
Figure 32: Mach contours (VL-1a).
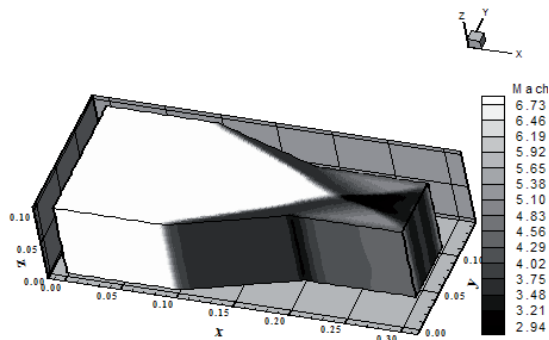
Figure 33: Mach contours (SW-2a-MIN).
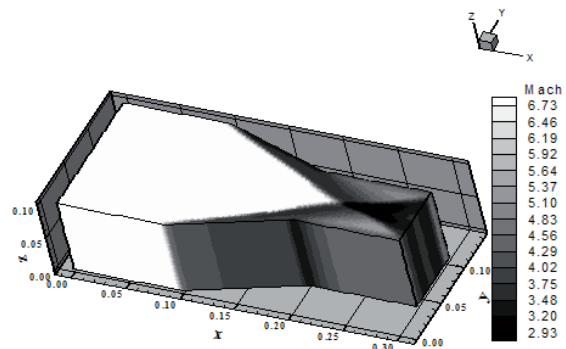
Figure 34: Mach contours (VL-2a-MIN).

Figure 37 exhibits the lower wall pressure distributions involving the Steger and Warming (1981) and the Van Leer (1982) schemes, in all their versions. The best compromise involving qualitative and quantitative features are observed with the Steger and Warming

(1981) TVD variant, with close pressure in comparison with the pressure plateau and appropriately pressure width at the ramp region (convergent region of the diffuser).
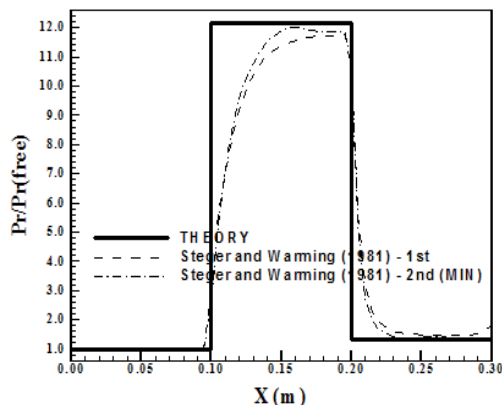
Figure 35: Wall pressure distributions (SW).
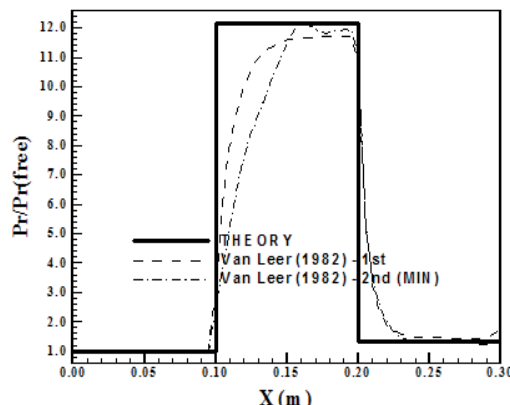
Figure 36: Wall pressure distributions (VL).
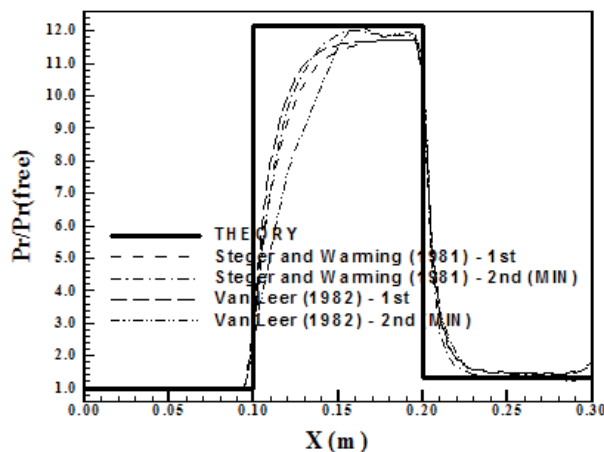
Figure 37: Wall pressure distributions involving SW and VL schemes.

Algorithm	Lower wall		Upper wall	
	β (°)	Error (%)	β (°)	Error (%)
Steger and Warming (1981) – 1a	28.0	1.818	28.6	4.000
Steger and Warming (1981) – 2a - MIN	27.2	1.091	27.7	0.727
Van Leer (1982) – 1a	28.0	1.818	28.9	5.091
Van Leer (1982) – 2a - MIN	27.0	1.818	28.2	2.545

Table 3: Shock angles of the oblique shock waves at lower and upper walls of the diffuser and percentage errors to each scheme.

Another way to check the accuracy of the Steger and Warming (1981) scheme and the Van Leer (1982) scheme in their two variants to this problem consists in determining the shock angle β of the oblique shock waves at the lower and upper walls of the diffuser. Following the same analysis described in the ramp problem, to $\phi = 20°$, angle of inclination of the convergent region of the diffuser and of the deflection of the flow after the shock wave, and to a freestream Mach number equals to 7.0, it is possible to find from Anderson Jr. (1984) the value $\beta = 27.5°$. Using a transfer in Figures 27 to 30, in the xy plane, it is possible to obtain the values of the oblique shock wave angles at the upper and lower walls and respective percentage errors shown in Tab. 3.

As can be observed from Table 3, the TVD version of the Steger and Warming (1981) scheme presents the best values to the shock angles of the oblique shock waves at the lower and upper wall of the diffuser in comparison with the others schemes, resulting in the best choice to this problem.

9.3 Numerical data of the simulations

Table 4 shows the numerical data of the simulations: maximum CFL number, number of iterations to convergence and computational cost of each scheme analyzed in this work.

Algorithm	Ramp		Diffuser		Cost[1]
	CFL	Iterations	CFL	iterations	
Steger and Warming (1981) – 1a	3.0	98	3.6	99	0.0000711
Steger and Warming (1981) - MIN	2.6	242	1.3	365	0.0000931
Van Leer (1982) – 1a	2.4	121	3.1	113	0.0000703
Van Leer (1982) – MIN	1.9	182	1.5	357	0.0000742

[1] Measured in seconds/per cell/per iteration.

Table 4: Numerical data of the simulations.

As can be observed from Table 4, the first order scheme of Van Leer (1982) is the cheapest, while the Steger and Warming (1981) TVD scheme using Minmod limiter is the most expensive. It is approximately 32.43% more expensive than the first order Van Leer (1982) scheme. It is possible to note that CFL numbers above 1.0 could be used, however, the maximum CFL number employed by all schemes was 3.6, which is still restrictive enough. One way to increase the maximum number of CFL to each scheme is the use of relaxation schemes, like Line Gauss-Seidel (LGS), which eliminates the error of the approximate factorization. This is the proposal to the next work involving implicit schemes by this author.

10 CONCLUSIONS

In the present work, the Steger and Warming (1981) and the Van Leer (1982) schemes are implemented, on a finite volume context and using a structured spatial discretization, to solve the Euler equations in the three-dimensional space. The Steger and Warming (1981) and the Van Leer (1982) schemes are flux vector splitting ones and in their original implementation are first order accurate. A MUSCL approach is implemented in these schemes aiming to obtain second order spatial accuracy. The Minmod non-linear limiter is employed to guarantee such accuracy and TVD high resolution properties. Both schemes are implemented following an implicit formulation. The flux vector splitting schemes employ approximate factorizations in ADI form. Both schemes are first order accurate in time. The algorithms are accelerated to the steady state solution using a spatially variable time step procedure, which has demonstrated effective gains in terms of convergence rate (Maciel, 2005 and 2008). Both schemes are applied to the solution of the physical problems of the supersonic flow along a ramp and the "cold gas" hypersonic flow along a diffuser.

The results have demonstrated that the most accurate results were obtained with the Steger and Warming (1981) TVD high resolution scheme. The Steger and Warming (1981) TVD scheme using Minmod limiter has yielded the most severe pressure field in the ramp problem, which indicates this one as a more conservative scheme to the prediction of moderate design conditions. The pressure distribution along the ramp was well predicted by both schemes. In the estimation of the angle of the oblique shock wave, both schemes presented appropriate predictions (errors less than 1.0%), with the exception of the first order

scheme of Van Leer (1982). In the diffuser problem, the most severe pressure field was estimated by the Van Leer (1982) TVD scheme, which indicates this scheme to more severe design conditions of aerospace vehicles. The lower wall pressure distribution was more appropriately described by the Steger and Warming (1981) scheme. In the prediction of the shock angles of the oblique shock waves at the lower and upper walls of the diffuser, the Steger and Warming (1981) TVD scheme was the best. In terms of computational cost, the Van Leer (1982) versions are cheaper than the Steger and Warming (1981) versions.

In terms of implicit numerical implementation, all schemes used CFL numbers in the range from 1.3 to 3.6, which indicates that the error introduced by the approximate factorization limits the rate of convergence of the schemes severely, although convergence in less than 100 iterations were obtained. A suggestion to improve the rate of convergence and to increase the range of CFL numbers consists in the use of relaxation schemes that eliminates the error of the approximate factorization. This is the objective of future works to be accomplished by this author, although other studies still with ADI schemes will be performed, with others schemes, aiming better evaluate the potential of this tool.

As final conclusion, the present author recommends the Steger and Warming (1981) TVD scheme to obtain more accurate solutions in the three-dimensional space. The Van Leer (1982) TVD scheme, due to its confirmed robustness and more conservative properties, could be used in the initial design phase of aerospace vehicles, where less refined results are characteristics.

11 ACKNOWLEDGEMENTS

REFERENCES

Anderson Jr., J. D., *Fundamentals of Aerodynamics*. McGraw-Hill, Inc., EUA, 563p, 1984.

Batina, J. T., Implicit Upwind Solution Algorithms for Three-Dimensional Unstructured Meshes. *AIAA Journal*, 31(5): 801-805, 1993

Beam, R. M., and Warming, R. F., An Implicit Factored Scheme for the Compressible Navier-Stokes Equations. *AIAA Journal*, 16(4): 393-402, 1978.

Douglas, J., On the Numerical Integration of $u_{xx}+u_{yy}=u_t$ by Implicit Methods. *Journal of the Society of Industrial and Applied Mathematics*, 3: 42-65, 1955

Douglas, J., and Gunn, J. E., A General Formulation of Alternating Direction Methods. *Numerische Mathematiks*, 6: 428-453, 1964.

Godunov, S. K., A Difference Scheme for Numerical Computation of Discontinuous Solution of Hydrodynamic Equations. Math. Sbornik, 47: 271-306, 1958.

Hirsch, C., *Numerical Computation of Internal and External Flows – Computational Methods for Inviscid and Viscous Flows*. John Wiley & Sons Ltd, 691p, 1990.

Jameson, A., and Mavriplis, D. J., Finite Volume Solution of the Two-Dimensional Euler Equations on a Regular Triangular Mesh. *AIAA Journal*, 24(4): 611-618, 1986.

Kutler, P., Computation of Three-Dimensional, Inviscid Supersonic Flows. *Lecture Notes in Physics*, 41: 287-374. Springer Verlag, Berlin, 1975.

Liou, M., and Steffen Jr., C. J., A New Flux Splitting Scheme. *Journal of Computational Physics*, 107: 23-39, 1993.

Maciel, E. S. G., Simulação Numérica de Escoamentos Supersônicos e Hipersônicos Utilizando Técnicas de Dinâmica dos Fluidos Computacional. *Doctoral Thesis*, ITA, São José dos Campos, SP, Brazil, 258p, 2002.

Maciel, E. S. G., Analysis of Convergence Acceleration Techniques Used in Unstructured Algorithms in the Solution of Aeronautical Problems – Part I. *Proceedings of the XVIII International Congress of Mechanical Engineering (XVIII COBEM)*, Ouro Preto, MG, Brazil, 2005.

Maciel, E. S. G., Analysis of Convergence Acceleration Techniques Used in Unstructured Algorithms in the Solution of Aeronautical Problems – Part II. *Proceedings of the XII Brazilian Congress of Thermal Engineering and Sciences (XII ENCIT)*, Belo Horizonte, MG, Brazil, 2008.

Peaceman, D. W., and Rachford, H. H., The Numerical Solution of Parabolic and Elliptic Differential Equations. *Journal of the Society of Industrial and Applied Mathematics*, 3: 28-41, 1955.

Radespiel, R., and Kroll, N., Accurate Flux Vector Splitting for Shocks and Shear Layers. *Journal of Computational Physics*, 121: 66-78, 1995.

Roe, P. L., Approximate Riemann Solvers, Parameter Vectors, and Difference Schemes. *Journal of Computational Physics*, 43: 357-372, 1981.

Steger, J. L., Implicit Finite-Difference Simulation of Flow About Arbitrary Two-Dimensional Geometries. *AIAA Journal*, 16(7): 679-686, 1978.

Steger, J. L., and Warming, R. F., Flux Vector Splitting of the Inviscid Gasdynamic Equations with Application to Finite-Difference Methods. *Journal of Computational Physics*, 40: 263-293, 1981.

Van Leer, B., Flux-Vector Splitting for the Euler Equations. *Lecture Notes in Physics*, 170: 507-512. Springer Verlag, Berlin, 1982.

Yanenko, N. N., *The Method of Fractional Steps*. Springer Verlag, NY, EUA, 1971.